J. Earth Planet. Sci. Nagoya Univ., Vol. 44, 89 to 102, 1997

Cambrian granulite to upper amphibolite facies metamorphism of post-797 Ma sediments in Madagascar

Masahiro ITO*, Kazuhiro SUZUKI and Setsuo YOGO****

**School of Informatics and Sciences, Nagoya University, Nagoya 464-01, Japan*
***Department of Earth and Planetary Sciences, Graduate School of Science, Nagoya University, Nagoya 464-01, Japan*
(Received November 6, 1997 / Accepted November 26, 1997)

ABSTRACT

The CHIME monazite and xenotime ages were determined for two paragneisses from Madagascar. The biotite-sillimanite-cordierite-quartz-microcline-plagioclase schist at Ihosy in southern Madagascar contains core-mantle monazite grains as well as chronologically unzoned ones. The unzoned monazite grains (8 of 11 analyzed grains) give a CHIME age of 527 ± 15 Ma. Two zoned grains show core ages of 1640 ± 180 and 797 ± 75 Ma with mantles of 550 ± 50 and 535 ± 10 Ma, respectively. The kyanite- and corundum-bearing cordierite-sillimanite-muscovite-biotite-plagioclase-quartz gneiss at Maevatanana in northwestern Madagascar contains both monazite and xenotime. Monazite and xenotime grains are chronologically uniform, and give CHIME ages of 534 ± 10 and 530 ± 32 Ma, respectively. These chronological data suggest that the high-grade paragneisses in Madagascar, if not all, formed through a single thermal event at ca. 530 Ma from post-797 Ma sediments. This metamorphism can be linked to the continental collision that resulted in Gondwana supercontinent.

INTRODUCTION

Gondwana supercontinent existed over 300 m.y. before its break-up in the Mesozoic. The evolution of this supercontinent, particularly of East Africa, Madagascar, Southern India, Sri Lanka and East Antarctica, was recently discussed on the basis of lithology, metamorphism and tectonics (e.g. Yoshida et al., 1992; Windley et al., 1994; Shiraishi et al., 1994; Kröner et al., 1996). The broad aspects of the picture for the Gondwana connection are generally agreed, but considerable debates still remain in detail, especially the location of the collision zone. Since Gondwana supercontinent formed through the late Cambrian (-latest Proterozoic) continental collision of East and West Gondwana, the distribution of Cambrian metamorphic rocks may play a key role in the analysis of the collision tectonics.

Recent geochronological studies have brought forth Cambrian metamorphic ages for high-grade paragneisses in the Kerala khondalite belt of southernmost India (Choudhary et al., 1992; Santosh et al., 1992; Bindu et al., 1996). Similar high-grade paragneisses are known to occur in Madagascar (Windley et al., 1994). Some of them were dated to be around 550 Ma (e.g. Kröner et al.,

1996, and their references). But little is known about the extension of the ca. 550 Ma metamorphic rocks in Madagascar. In order to shed more light on the collision tectonics of Gondwana, we have made the CHIME dating of monazite and xenotime from two samples of high-grade paragneisses from Madagascar.

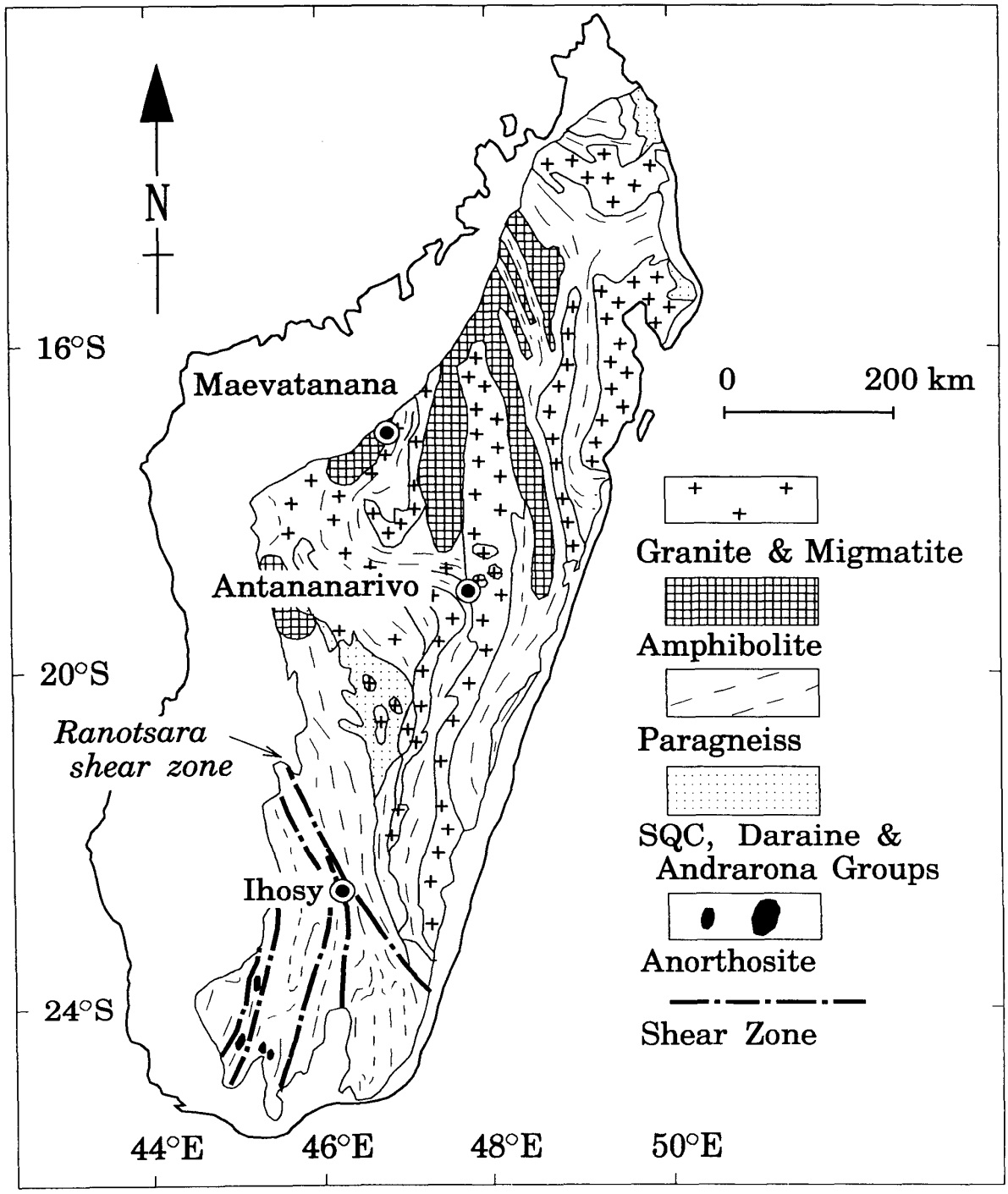

Fig. 1. Simplified and schematic geologic map showing the main basements of Madagascar (from Windley et al., 1994).

GENERAL GEOLOGY AND SAMPLE DESCRIPTION

The basement rocks in Madagascar are divided into the southern and central-northern sectors by the northwest trending Ranotsara shear zone (Windley et al., 1994; Fig. 1). The southern sector consists predominantly of high-grade metamorphic rocks formed under the granulite and upper amphibolite facies conditions. Particularly common are cordierite- and sillimanite-bearing paragneisses with intercalated marble, metaquartzite and amphibolite layers. They generally trend in NS direction. The central-northern sector is underlain mainly by granitoids and amphibolite (greenstone belt) with a subordinate amount of paragneiss. This sector is traversed by a north-trending 100—150 km wide dextral shear zone of probable Pan-African age; the western margin of the shear zone runs through around Antananarivo. Rocks in the dextral shear zone were metamorphosed under the granulite and upper amphibolite facies conditions, and include reworked older basement. Two paragneiss samples were collected for the present CHIME dating; biotite-sillimanite-cordierite gneiss from Ihosy in the southern sector and kyanite- and corundum-bearing cordierite-sillimanite-muscovite-biotite gneiss from Maevatanana in the western part of the central-northern sector.

Biotite-sillimanite-cordierite-quartz-microcline-plagioclase gneiss from Ihosy

This rock is composed of plagioclase, microcline, quartz, biotite, cordierite, sillimanite and opaque mineral, together with small amounts of zircon, apatite and monazite. Plagioclase, sodic oligoclase in composition, is granoblastic and is slightly sericitized. Biotite, sillimanite and quartz together with fluid inclusions are found within plagioclase grains. Myrmekite is rarely developed. Microcline is commonly string and film perthite with well-developed microcline twinning. It includes sillimanite and plagioclase. Quartz shows often undulatory extinction and includes sillimanite, biotite, plagioclase, microcline, apatite and opaque mineral. Cordierite occurs as granoblastic grains with inclusions of sillimanite, biotite, quartz and opaque mineral. Some cordierite grains are twinned. It is slightly altered. Sillimanite is coarse-grained, sometimes euhedral or subhedral, and includes quartz, biotite, zircon and opaque mineral. It shows often undulatory extinction. The sillimanite inclusions in cordierite, quartz and biotite are of small and short prismatic form, and are frequently oriented. Biotite is oriented along the schistosity. It is pleochroic; X = nearly colourless, Y = brown and Z = light brown. Symplectic biotite is also found. Inclusions in biotite are sillimanite, apatite, zircon, monazite, and opaque mineral. Muscovite is very small in amount, and may be derived from the alteration of plagioclase. Monazite is anhedral, and ranges in size from 0.02 to 0.15 mm.

Kyanite- and corundum-bearing cordierite-sillimanite-muscovite-biotite-plagioclase-quartz gneiss from Maevatanana

Biotite-rich layers are finely alternated with feldspathic layers which are somewhere coarse-grained. This rock is composed of plagioclase, quartz,

biotite, muscovite, cordierite and sillimanite together with accessory corundum, kyanite, zircon, apatite, monazite, xenotime and opaque mineral. Plagioclase (oligoclase) is granoblastic and is slightly sericitized. It includes biotite, sillimanite, muscovite and zircon. Quartz is also granoblastic with inclusions of biotite, sillimanite and muscovite. Biotite is commonly associated with muscovite and sillimanite. It is pleochroic; X = nearly colourless, Y = yellowish olive green and Z = olive green. Inclusions in biotite are apatite, zircon, monazite and opaque mineral. Sillimanite is fibrous to very long prismatic, intimately intergrown with muscovite and biotite. Cordierite is granoblastic with inclusions of biotite, sillimanite and opaque mineral. It is moderately, sometimes completely, altered. Muscovite flakes include plagioclase, quartz, biotite, sillimanite, corundum and kyanite. Corundum and kyanite are always coated with muscovite. Monazite and xenotime occur as tiny grains, but exceptionally large grains exceed 0.04 mm in size.

CHIME AGES

Monazite and xenotime grains in polished thin sections, prepared for the conventional electron microprobe analyses, were analyzed on JEOL JXA-733 electron microprobe equipped with three wavelength dispersive-type spectrometers. Instrument operating conditions were 15 kv accelerating voltage, 0.02—0.15 μA current and 5 μm probe diameter. X-ray intensities were integrated 200s for the lines and 100s for backgrounds at two optimum positions on both sides of the lines. The detection limits of ThO_2, UO_2 and PbO at 2 σ confidence level are 0.012, 0.007 and 0.004 wt.%, respectively, and possible errors in the determination of ThO_2, UO_2 and PbO are about 14% for 0.1 wt.% of the concentrations. The analytical results are listed in Table 1. CHIME ages were calculated through the method described by Suzuki and Adachi (1991a,b, 1994), Adachi and Suzuki (1992) and Suzuki et al. (1994).

Biotite-sillimanite-cordierite-quartz-microcline-plagioclase gneiss from Ihosy

Eleven monazite grains were analyzed. Nine of these grains are chronologically unzoned, and two grains show a core-mantle relation. Figure 2 shows the PbO vs. ThO_2* plots of chronologically unzoned monazite grains. Data points, except those for grain margins (open circle), are arrayed linearly on the diagram. They are regressed with an isochron of 527 ± 15 Ma (MSWD = 0.28) with an intercept value of -0.0010 ± 0.0045.

Figures 3a shows the PbO vs. ThO_2* plots of analytical data of a core-mantle monazite grain (M02). Data points for the core (solid square) and the mantle (solid circle) are separately arrayed, and define different isochrons of 1640 ± 180 Ma (MSWD = 0.66) and 550 ± 50 Ma, respectively. Data points between the 1640 and 550 Ma isochrons (open square, cross and triangle) are for the core-mantle boundary region, but do not define either a certain area in the cross section or any isochrons. The textural feature suggests an overlap of the 550 Ma mantle on the 1640 Ma core at analyzed points on the cross

Table 1. Microprobe analyses of ThO_2, UO_2 and PbO of monazite (M) and xenotime (X) from metamorphic rocks at Ihosy and Maevatanana, Madagascar.

Spot No.	ThO2 (wt.%)	UO2 (wt.%)	PbO (wt.%)	Age (Ma)	ThO2* (wt.%)
Biotite-sillimanite-cordierite gneiss (Ihosy)					
M01-01	6.38	0.084	0.149	525	6.66
M01-02	6.32	0.049	0.147	534	6.48
M01-03	6.43	0.079	0.152	532	6.70
M01-04	5.30	0.175	0.134	534	5.88
M01-05	6.24	0.145	0.144	503	6.72
M01-06	5.73	0.170	0.139	517	6.29
M01-07 r	5.46	0.117	0.120	482	5.84
M01-08 r	5.47	0.174	0.119	462	6.05
M01-09 r	5.67	0.170	0.129	488	6.23
M01-10 r	5.63	0.207	0.126	469	6.31
M01-11 r	5.75	0.191	0.130	479	6.38
M02-01 4030	6.98	0.348	0.574	1592	8.25
M02-02 4033	7.26	0.245	0.572	1605	8.15
M02-03 4038	7.29	0.246	0.587	1638	8.19
M02-04 4041	7.48	0.276	0.568	1534	8.48
M02-05 2034	7.09	0.335	0.510	1415	8.28
M02-06 4628	6.06	0.143	0.194	693	6.54
M02-07 5330	6.72	0.112	0.163	538	7.09
M02-08 2510	6.80	0.114	0.157	515	7.17
M02-09 1349	6.72	0.138	0.164	536	7.18
M02-10 5343	6.82	0.154	0.169	541	7.34
M02-11 0236	6.31	0.174	0.135	460	6.88
M02-12 0826	6.21	0.143	0.130	458	6.68
M02-13 0836	6.15	0.150	0.150	530	6.65
M02-14 0641	6.00	0.123	0.133	488	6.41
M02-15 0852	5.67	0.170	0.139	524	6.23
M02-16 1417	5.57	0.141	0.131	510	6.04
M02-17 1425	5.26	0.133	0.131	540	5.70
M02-18 1433	5.53	0.097	0.127	511	5.85
M02-19 1453	5.52	0.148	0.130	509	6.01
M02-20 1459	5.25	0.127	0.119	495	5.67
M02-21 2206	5.50	0.133	0.129	509	5.94
M02-22 2212	5.56	0.124	0.137	539	5.97
M02-23 2219	5.69	0.100	0.129	503	6.02
M02-24 2224	4.10	0.040	0.119	658	4.24
M02-25 2238	5.40	0.247	0.438	1590	6.30
M02-26 2254	5.72	0.129	0.143	546	6.15
M02-27 2259	5.12	0.137	0.113	477	5.57
M02-28 3001	5.76	0.106	0.127	489	6.11
M02-29 3007	5.76	0.082	0.127	496	6.03
M02-30 3013	5.72	0.101	0.139	538	6.05
M02-31 3020	5.47	0.098	0.131	529	5.80
M02-32 3026	5.84	0.382	0.528	1667	7.24
M02-33 3031	5.42	0.591	0.546	1647	7.58
M02-34 3038	6.10	0.271	0.503	1624	7.09
M02-35 3043	6.17	0.228	0.491	1604	7.00
M02-36 3049	5.58	0.166	0.276	1039	6.16
M02-37 3057	5.59	0.135	0.136	529	6.04
M02-38 3063	5.80	0.136	0.142	533	6.25
M02-39 3069	5.69	0.170	0.124	468	6.25
M02-40 3601	5.74	0.089	0.133	519	6.03
M02-41 3609	5.51	0.102	0.134	538	5.85
M02-42 3616	6.28	0.153	0.174	600	6.79
M02-43 3625	5.62	0.225	0.461	1634	6.44
M02-44 3631	5.53	0.302	0.471	1622	6.64
M02-45 3637	5.10	0.637	0.511	1577	7.42
M02-46 3644	6.03	0.237	0.449	1497	6.89
M02-47 3651	6.04	0.112	0.163	597	6.41
M02-48 3657	5.65	0.135	0.138	531	6.10
M02-49 3663	5.74	0.139	0.137	519	6.19
M02-50 3669	5.52	0.167	0.112	434	6.07
M02-51 4305	6.61	0.112	0.163	546	6.98
M02-52 4311	6.43	0.119	0.151	520	6.82
M02-53 4319	5.90	0.169	0.149	540	6.46
M02-54 4336	5.42	0.254	0.306	1125	6.31
M02-55 4345	5.54	0.107	0.130	519	5.90
M02-56 4351	5.61	0.105	0.137	540	5.96
M02-57 4357	5.54	0.132	0.134	527	5.98
M02-58 4366	5.48	0.177	0.116	448	6.06
M02-59 5014	5.46	0.124	0.121	485	5.87
M02-60 5023	4.15	0.093	0.103	541	4.46
M02-61 5037	5.28	0.108	0.126	527	5.64
M02-62 5049	5.62	0.137	0.137	530	6.07
M02-63 5056	5.48	0.251	0.143	532	6.31
M02-64 5809	5.73	0.150	0.118	446	6.23
M02-65 5823	5.27	0.128	0.122	505	5.69
M02-66 5840	5.81	0.153	0.128	476	6.31
M02-67 6415	5.63	0.142	0.140	538	6.10
M02-68 6425	5.71	0.136	0.126	480	6.15
M02-69 6429	5.95	0.152	0.121	442	6.46
M02-70 6436	3.05	0.765	0.102	432	5.56
M02-71 6728	5.80	0.162	0.142	526	6.33
M02-72 4645	5.75	0.113	0.137	524	6.12
M02-73 4045	5.85	0.125	0.140	524	6.26
M02-74 3345	6.60	0.253	0.545	1655	7.53
M02-75 2445	5.59	0.148	0.136	526	6.08
M02-76 1945	5.77	0.133	0.134	508	6.21
M02-77 2152	5.98	0.157	0.149	538	6.50
M02-78 2752	5.65	0.123	0.132	510	6.06
M02-79 3252	5.89	0.173	0.233	840	6.48
M02-80 3752	5.76	0.121	0.142	542	6.16

Table 1. (continued).

Spot No.	ThO2 (wt.%)	UO2 (wt.%)	PbO (wt.%)	Age (Ma)	ThO2* (wt.%)
M02-81 4352	5.93	0.104	0.136	511	6.27
M02-82 4362	5.80	0.141	0.140	524	6.27
M02-83 3762	5.78	0.133	0.144	542	6.22
M02-84 3262	5.77	0.140	0.138	520	6.24
M02-85 2538	5.95	0.194	0.473	1623	6.66
M02-86 2530	6.15	0.308	0.509	1602	7.27
M02-87 2030	5.52	0.567	0.480	1457	7.56
M03-01	5.48	0.122	0.131	525	5.88
M03-02	5.72	0.168	0.136	509	6.28
M03-03	5.56	0.188	0.134	511	6.18
M03-04	5.35	0.177	0.140	554	5.94
M03-05	5.66	0.149	0.142	540	6.16
M04-01	5.68	0.172	0.138	519	6.25
M04-02	5.59	0.191	0.138	519	6.22
M04-03	5.58	0.177	0.143	544	6.17
M04-04	5.60	0.159	0.134	515	6.12
M04-05	5.65	0.171	0.131	495	6.21
M04-06	5.55	0.177	0.145	554	6.14
M04-07	5.77	0.199	0.134	491	6.42
M04-08	5.69	0.172	0.143	535	6.26
M04-09	5.73	0.206	0.144	526	6.41
M04-10	5.65	0.192	0.145	540	6.29
M05-01	2.90	0.328	0.083	492	3.98
M05-02	3.08	0.237	0.091	552	3.87
M05-03	2.97	0.252	0.081	502	3.80
M05-04	3.26	0.261	0.093	528	4.13
M05-05	3.31	0.274	0.094	521	4.22
M06-01	7.52	0.139	0.178	525	7.98
M06-02	7.56	0.124	0.187	550	7.97
M06-03	7.45	0.204	0.178	515	8.13
M06-04	7.53	0.154	0.181	529	8.04
M06-05	7.45	0.126	0.178	530	7.87
M07-01	6.85	0.163	0.163	518	7.40
M07-02	6.25	0.140	0.155	540	6.71
M08-01 r	6.66	0.120	0.140	468	7.06
M08-02	7.03	0.141	0.158	496	7.49
M08-03	6.96	0.123	0.165	524	7.37
M08-04	6.67	0.125	0.153	509	7.08
M08-05	7.00	0.120	0.163	518	7.39
M08-06	6.84	0.124	0.155	503	7.25
M08-07	6.63	0.128	0.162	539	7.05
M08-08	6.75	0.130	0.160	525	7.18
M08-09	6.70	0.137	0.161	529	7.15
M08-10	6.45	0.144	0.157	532	6.92
M08-11	6.63	0.136	0.146	485	7.08
M08-12	6.74	0.126	0.163	533	7.16

Spot No.	ThO2 (wt.%)	UO2 (wt.%)	PbO (wt.%)	Age (Ma)	ThO2* (wt.%)
M08-13	6.74	0.131	0.161	526	7.17
M08-14	6.88	0.141	0.156	498	7.35
M08-15	6.69	0.138	0.155	510	7.15
M08-16	6.67	0.136	0.159	523	7.12
M08-17	6.63	0.144	0.152	502	7.11
M08-18	6.81	0.126	0.164	534	7.23
M08-19	6.63	0.123	0.157	525	7.04
M08-20	6.77	0.128	0.157	513	7.20
M09-01	6.41	0.167	0.154	521	6.96
M09-02	6.45	0.161	0.150	503	6.98
M09-03	6.55	0.181	0.161	528	7.15
M09-04	6.53	0.158	0.163	542	7.06
M09-05	6.46	0.163	0.155	521	7.00
M09-06	6.44	0.142	0.151	513	6.91
M09-07	6.39	0.173	0.159	537	6.96
M09-08	6.27	0.141	0.153	532	6.74
M09-09	5.60	0.185	0.140	529	6.22
M09-10	6.56	0.175	0.160	527	7.14
M09-11	6.42	0.165	0.161	543	6.97
M09-12	6.61	0.146	0.156	518	7.10
M09-13	6.48	0.176	0.161	535	7.06
M09-14	5.85	0.191	0.148	537	6.48
M09-15	5.64	0.200	0.142	529	6.31
M10-01	7.25	0.136	0.170	518	7.70
M10-02	10.5	0.195	0.253	531	11.2
M10-03	13.0	0.233	0.313	534	13.8
M10-04	9.00	0.157	0.206	509	9.52
M10-05	9.05	0.150	0.216	531	9.55
M10-06	9.07	0.166	0.216	526	9.62
M10-07	6.45	0.176	0.160	534	7.03
M10-08	6.50	0.170	0.152	505	7.06
M10-09	6.55	0.120	0.152	515	6.95
M10-10	6.67	0.119	0.155	517	7.07
M10-11	6.69	0.165	0.162	526	7.24
M10-12 r	6.58	0.125	0.137	460	7.00
M10-13	5.93	0.140	0.143	526	6.40
M10-14	5.50	0.150	0.135	531	5.99
M10-15	6.22	0.137	0.147	519	6.67
M10-16	5.93	0.153	0.147	536	6.43
M10-17	6.58	0.123	0.160	537	6.99
M10-18	11.6	0.181	0.273	527	12.2
M10-19	5.36	0.140	0.127	510	5.83
M10-20	5.71	0.142	0.140	533	6.18
M10-21	5.77	0.147	0.139	523	6.26
M10-22	4.94	0.148	0.124	537	5.43
M10-23	6.34	0.169	0.157	533	6.90

Table 1. (continued).

Spot No.	ThO2 (wt.%)	UO2 (wt.%)	PbO (wt.%)	Age (Ma)	ThO2* (wt.%)
M10-24	4.49	0.321	0.126	531	5.56
M10-25	6.31	0.132	0.149	518	6.75
M10-26	7.21	0.163	0.173	526	7.74
M10-27 r	6.44	0.387	0.155	471	7.71
M10-28	6.64	0.115	0.160	536	7.02
M10-29	6.63	0.139	0.159	525	7.09
M10-30	5.19	0.687	0.169	532	7.47
M11-01 0632	6.64	0.181	0.163	530	7.24
M11-02 0638	6.66	0.185	0.161	520	7.27
M11-03 0646	6.29	0.166	0.152	523	6.83
M11-04 0654	5.97	0.192	0.149	531	6.60
M11-05 0051	5.27	0.429	0.144	507	6.69
M11-06 1030	6.64	0.159	0.160	523	7.17
M11-07 1034	6.64	0.145	0.158	522	7.12
M11-08 1043	6.67	0.164	0.164	533	7.21
M11-09 1051	6.36	0.169	0.158	535	6.92
M11-10 1056	6.06	0.168	0.157	557	6.62
M11-11 1814	6.69	0.097	0.140	470	7.01
M11-12 1819	6.76	0.118	0.164	539	7.15
M11-13 1829	7.07	0.134	0.167	522	7.51
M11-14 1837	7.21	0.131	0.174	534	7.64
M11-15 1844	7.21	0.116	0.179	553	7.59
M11-16 1855	6.48	0.161	0.163	544	7.02
M11-17 1861	6.67	0.158	0.167	546	7.19
M11-18 1869	4.63	0.143	0.106	488	5.10
M11-19 2608	6.80	0.156	0.160	512	7.31
M11-20 2615	7.25	0.124	0.173	529	7.66
M11-21 2621	7.07	0.125	0.173	543	7.49
M11-22 2632	7.06	0.131	0.173	541	7.49
M11-23 2641	7.68	0.116	0.183	534	8.07
M11-24 2648	7.06	0.104	0.171	541	7.41
M11-25 2655	6.61	0.119	0.160	536	7.00
M11-26 2663	6.58	0.170	0.158	518	7.15
M11-27 2671	4.96	0.343	0.140	539	6.10
M11-28 3506	7.05	0.134	0.174	545	7.50
M11-29 3513	7.23	0.121	0.176	541	7.63
M11-30 3521	7.36	0.077	0.173	532	7.62
M11-31 3529	7.56	0.126	0.183	538	7.98
M11-32 3536	7.62	0.140	0.184	534	8.08
M11-33 3543	7.74	0.327	0.203	541	8.83
M11-34 3553	7.32	0.103	0.173	529	7.66
M11-35 4300	7.30	0.121	0.157	481	7.69
M11-36 4322	7.50	0.128	0.182	541	7.92
M11-37 4340	8.23	0.453	0.230	556	9.73
M11-38 4349	7.03	0.306	0.179	521	8.05
M11-39 4357	7.69	0.124	0.185	537	8.10
M11-40 4364	3.75	0.079	0.0917	537	4.01
M11-41 5103	7.25	0.131	0.177	541	7.68
M11-42 5107	7.58	0.138	0.184	536	8.04
M11-43 5121	8.46	0.117	0.203	538	8.85
M11-44 5135	10.5	0.384	0.411	813	11.8
M11-45 5143	8.86	0.500	0.243	542	10.5
M11-46 5151	8.16	0.275	0.205	532	9.07
M11-47 5158	8.03	0.146	0.196	541	8.51
M11-48 5164	6.79	0.157	0.169	544	7.31
M11-49 6002	7.19	0.126	0.173	533	7.61
M11-50 6013	8.31	0.132	0.201	539	8.75
M11-51 6026	10.7	0.371	0.408	795	12.0
M11-52 6033	10.4	0.346	0.393	792	11.6
M11-53 6044	8.29	0.141	0.199	535	8.76
M11-54 6053	8.17	0.137	0.198	539	8.63
M11-55 6060	7.01	0.151	0.171	535	7.51
M11-56 6064	5.03	0.150	0.128	545	5.52
M11-57 6903	8.46	0.141	0.204	536	8.93
M11-58 6911	7.79	0.108	0.184	531	8.15
M11-59 6917	11.0	0.358	0.420	801	12.2
M11-60 6926	9.70	0.320	0.371	804	10.8
M11-61 6935	8.34	0.129	0.201	539	8.76
M11-62 6942	8.09	0.132	0.191	525	8.52
M11-63 6949	8.20	0.132	0.195	531	8.63
M11-64 6955	7.64	0.139	0.187	542	8.10
M11-65 6961	2.22	0.245	0.0709	549	3.03
M11-66 7809	7.74	0.126	0.183	528	8.15
M11-67 7817	9.33	0.358	0.360	798	10.5
M11-68 7825	9.35	0.366	0.365	805	10.6
M11-39 7833	8.84	0.326	0.343	803	9.95
M11-70 7841	8.67	0.151	0.209	534	9.17
M11-71 7849	7.97	0.130	0.188	527	8.40
M11-72 7856	3.85	0.309	0.114	549	4.88
M11-73 8815	11.0	0.347	0.277	534	12.2
M11-74 8820	9.10	0.387	0.237	536	10.4
M11-75 8833	11.0	0.422	0.284	539	12.4
M11-76 8839	8.98	0.218	0.221	535	9.70
M11-77 8844	6.39	0.172	0.161	542	6.96
M11-78 8850	2.32	0.261	0.0729	537	3.19
M11-79 9628	6.56	0.254	0.170	539	7.40
M11-80 9633	5.61	0.247	0.146	535	6.42
M11-81 9638	5.82	0.425	0.164	534	7.23
M11-82 9641	4.28	0.465	0.138	556	5.82

Table 1. (continued).

Spot No.	ThO2 (wt.%)	UO2 (wt.%)	PbO (wt.%)	Age (Ma)	ThO2* (wt.%)
Kyanite- and corundum-bearing cordierite-sillimanite-muscovite gneiss (Maevatanana)					
M01-01	10.7	1.34	0.350	544	15.1
M01-02	10.8	1.31	0.342	531	15.1
M01-03	10.4	1.19	0.323	529	14.3
M01-04	10.6	0.890	0.308	534	13.5
M01-05	11.1	1.13	0.343	542	14.9
M01-06	13.9	0.787	0.378	537	16.5
M01-07	12.9	0.787	0.361	545	15.5
M01-08	11.7	0.769	0.327	540	14.2
M01-09	10.2	0.974	0.306	537	13.4
M01-10	10.8	1.23	0.339	536	14.9
M01-11	12.9	0.941	0.364	532	16.1
M01-12	16.0	0.655	0.417	538	18.2
M01-13	8.88	0.599	0.251	542	10.9
M01-14	13.6	1.06	0.396	543	17.1
M01-15	11.4	0.781	0.318	535	14.0
M01-16	13.0	1.34	0.394	533	17.4
M01-17	10.8	1.37	0.352	539	15.3
M02-01	11.6	0.938	0.332	532	14.7
M02-02	11.8	0.941	0.339	533	14.9
M02-03	12.0	0.932	0.338	529	15.0
M02-04	7.09	1.28	0.259	536	11.3
M02-05	10.9	1.05	0.324	532	14.3
M02-06	10.3	1.12	0.320	536	14.0
M02-07	9.58	1.50	0.331	534	14.5
M02-08	9.81	1.59	0.343	535	15.1
M02-09	8.97	1.36	0.305	530	13.5
M02-10	7.31	1.52	0.281	535	12.4
M02-11	8.05	1.46	0.290	528	12.9
M02-12	7.85	0.776	0.236	531	10.4
M02-13	6.85	0.560	0.202	544	8.71
M02-14	9.36	1.07	0.295	537	12.9
M02-15	8.11	1.42	0.291	532	12.8
M02-16	9.02	1.45	0.313	531	13.8
M02-17	8.90	1.44	0.310	532	13.7
M02-18	11.9	0.904	0.333	527	14.8
M02-19	12.2	0.758	0.334	532	14.8
M02-20	12.0	0.869	0.343	541	14.9
M02-21	11.6	1.02	0.339	531	15.0
M02-22	8.84	1.33	0.300	533	13.2
M02-23	11.4	1.03	0.337	535	14.8
M02-24	10.6	1.24	0.341	545	14.7
M02-25	11.3	1.06	0.335	530	14.9

Spot No.	ThO2 (wt.%)	UO2 (wt.%)	PbO (wt.%)	Age (Ma)	UO2* (wt.%)
X01-01	0.411	1.49	0.123	545	1.61
X01-02	0.477	1.64	0.136	542	1.79
X01-03	0.482	2.06	0.166	537	2.21
X01-04	0.397	1.41	0.112	521	1.53
X01-05	0.285	1.17	0.093	532	1.26
X01-06	0.132	1.25	0.097	538	1.29
X01-07	0.142	1.19	0.093	541	1.23
X01-08	0.148	1.13	0.088	532	1.18
X01-09	0.239	1.26	0.103	548	1.33
X01-10	0.439	1.82	0.148	540	1.95
X01-11	0.390	1.46	0.117	533	1.57
X01-12	0.373	1.71	0.136	534	1.82
X01-13	0.364	1.37	0.113	545	1.48
X02-01	0.216	1.41	0.115	556	1.47
X02-02	0.203	1.27	0.102	546	1.33
X02-03	0.153	1.58	0.118	522	1.62
X02-04	0.128	1.49	0.112	525	1.53
X02-05	0.278	1.66	0.132	541	1.74
X02-06	0.342	1.32	0.107	535	1.43

Note

ThO_2*: sum of the measured ThO_2 and ThO_2 equivalent of the measured UO_2.

UO_2*: sum of the measured UO_2 and UO_2 equivalent of the measured ThO_2.

Age: apparent age calculated through equation 1 of Suzuki and Adachi (1991a,b, 1994), Suzuki et al. (1994) and Adachi and Suzuki (1992).

r: rim

Analized position is shown for M02 and M11 monazite grains: for example, M02-01 4030 means 40μm from right and 30μm from top.

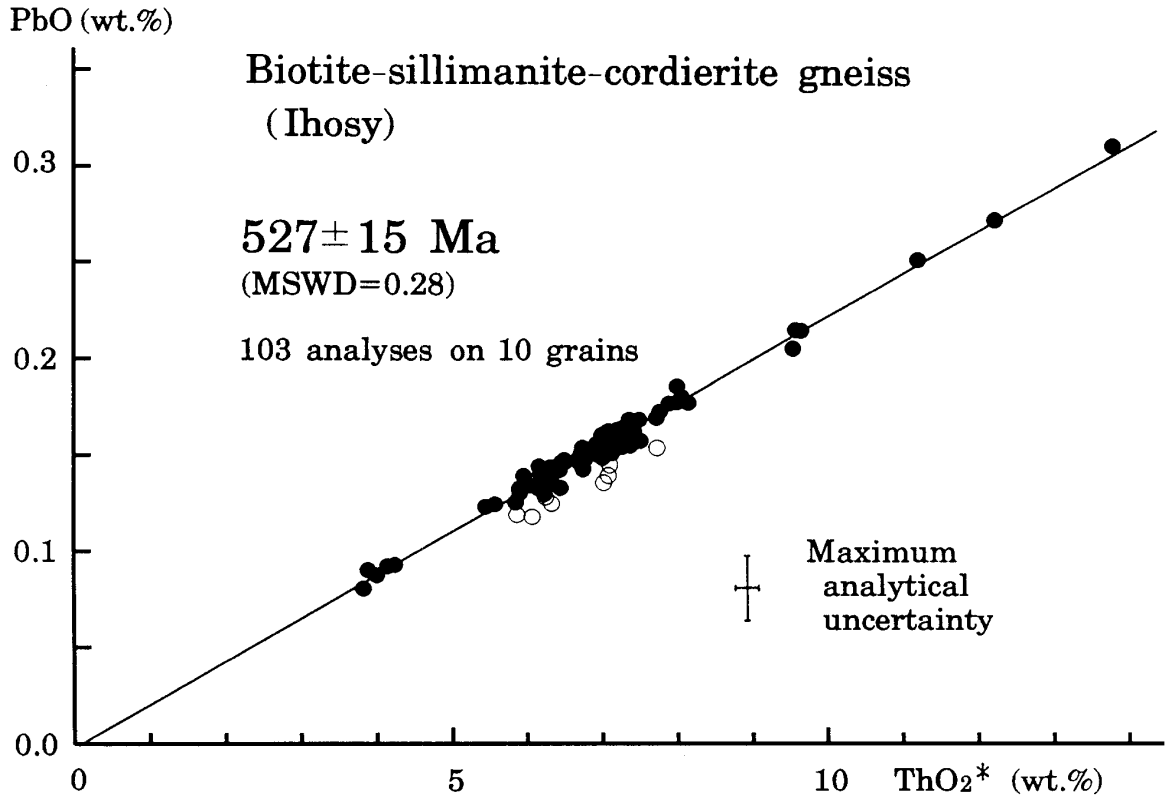

Fig. 2. Plot of PbO vs. ThO_2* for unzoned monazite grains from biotite-sillimanite-cordierite gneiss from Ihosy. Open circle represents data points for grain margins. Error bars in the figure represent 2 σ analytical uncertainty, and error quoted in age is of 2 σ.

section. Data points (open circle) below the 550 Ma isochron may result from Pb loss.

Figure 3b shows the PbO vs. ThO_2* plots of analytical data of a core-mantle monazite grain (M11). Within this grain UO_2 is heterogeneously distributed with respect to the shape of the cross section, showing a homogeneous concentration (0.320—0.384 wt.%) in the core and variable concentrations (0.077—0.500 wt.%) in the mantle. The ThO_2 content of the core (8.843—11.04 wt.%) is higher than that of the mantle (2.22—11.03 wt.% and mostly in the range between 6.5 and 8.5 wt.%). This compositional discontinuity suggests overgrowth of the mantle under a different chemical environment. The CHIME ages are 797 ± 75 Ma for the core and 535 ± 10 Ma for the mantle.

Kyanite- and corundum-bearing cordierite-sillimanite-muscovite-biotite-plagioclase-quartz gneiss from Maevatanana

Most monazite grains from this sample are very small in size, but two grains have a size sufficient for microprobe analyses. Seventeen spots were measured on M01-grain and 25 spots on M02-grain. The ThO_2 and UO_2 distributions are highly variable within individual grains (Table 1), but data points are arrayed linearly on the PbO vs. ThO_2* diagram (Fig. 4a). The best

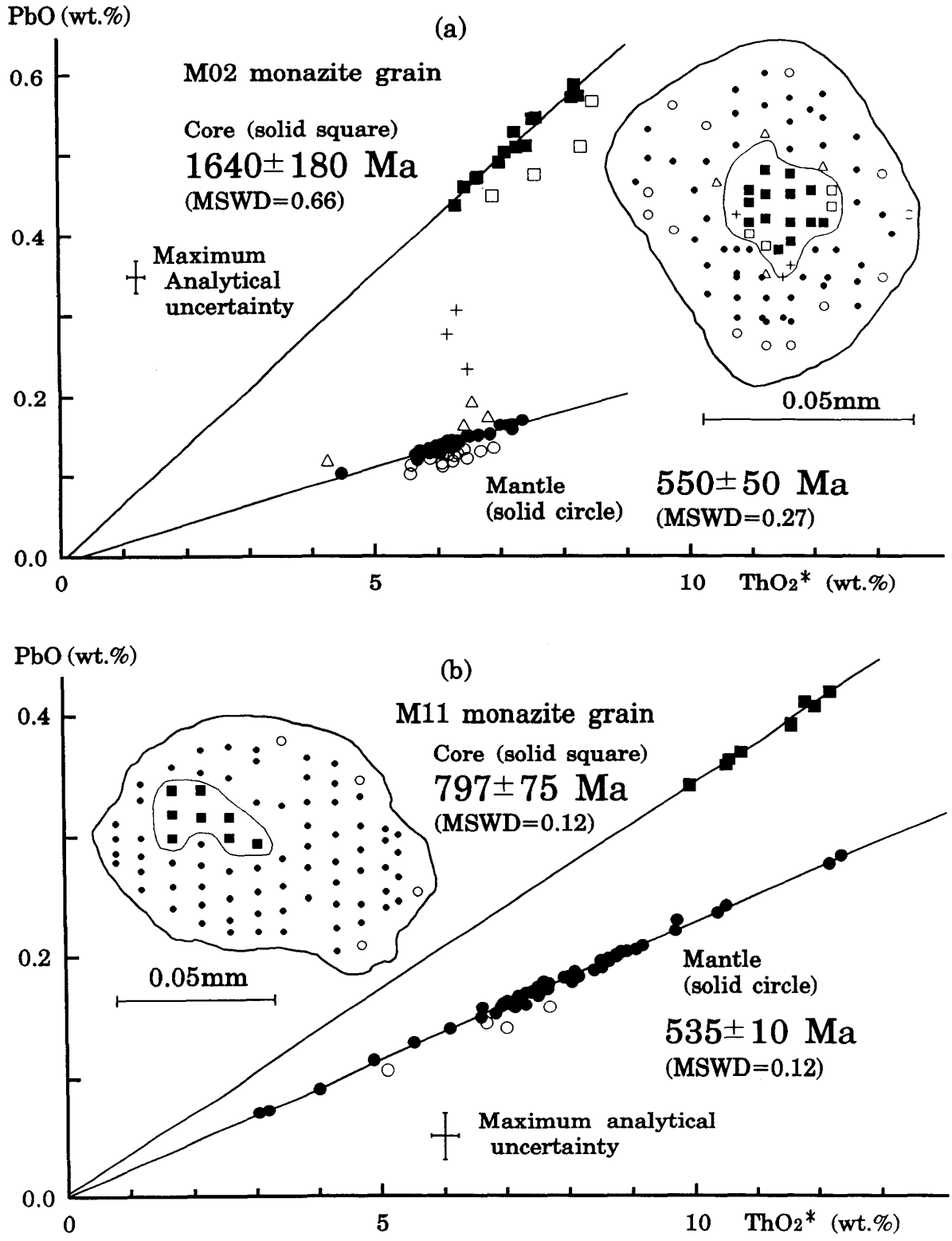

Fig. 3. Plot of PbO vs. ThO_2* for core-mantle monazite grains M02 (a) and M11(b) from biotite-sillimanite-cordierite gneiss from Ihosy. Solid square represents data points for the core and solid circle represents those for the mantle. Data points for grain margin are shown with open circle, and those for the core-mantle boundary with open square and cross. Explanation for errors is the same as Fig. 2.

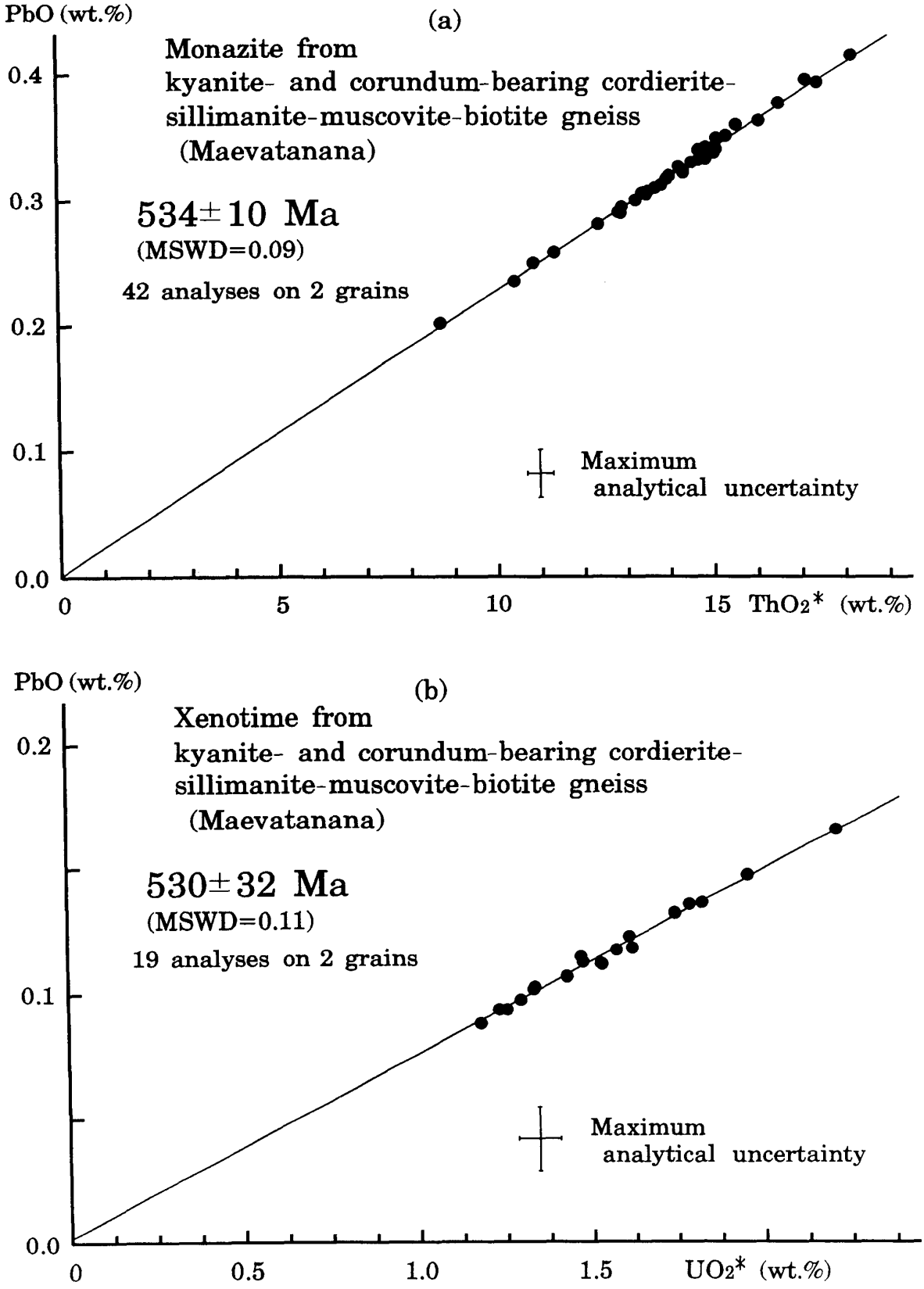

Fig. 4. Plot of PbO vs. ThO_2* for monazite (a) and that of PbO vs. UO_2* for xenotime (b) from kyanite- and corundum-bearing cordierite-sillimanite-muscovite-biotite gneiss from Maevatanana. Explanation for errors is the same as Fig. 2.

fit regression line yields an age of 534 ± 10 Ma (MSWD = 0.09) and an intercept value of 0.0010 ± 0.0062. Figure 4b shows the PbO vs. UO_2 plots of 19 analytical data for two xenotime grains. All data points are arrayed linearly, and define an isochron of 530 ± 32 Ma (MSWD = 0.11) with an intercept value of 0.0019 ± 0.0072. Despite the detailed microprobe analysis, no age signature older than ca. 530 Ma can be obtained on both the monazite and xenotime grains.

DISCUSSION AND CONCLUSION

The CHIME dating disclosed that the biotite-sillimanite-cordierite gneiss from Ihosy contains chronologically zoned monazite grains as well as unzoned ones. The core ages are 1640 ± 180 and 797 ± 75 Ma, although the mantles and unzoned grains give unequivocal ages of 527—550 Ma. The zoning pattern coupled with the considerable difference in core ages suggests that the older core are of detrital origin, retaining pre-metamorphic information. Inheritance of monazite grains in the uppermost amphibolite to granulite facies paragneisses is not uncommon (Parrish, 1990; Suzuki and Adachi, 1994; Suzuki et al., 1994). Thus, we conclude that the biotite-sillimanite-cordierite gneiss at Ihosy formed through the ca. 530 (527—550) Ma single metamorphic event from a post-795 ± 75 Ma sediment. This reinforces the previous age assignment of late Proterozoic (< ca. 720 Ma) sedimentation and ca. 550 Ma metamorphism for the gneisses exposed at Ihosy (Kröner et al., 1996).

The sample of kyanite- and corundum-bearing cordierite-sillimanite-muscovite-biotite gneiss was collected from the metamorphic sequence peripheral to the Maevatanana greenstone belt of possible Archean age. The nature of the boundary between the peripheral rocks and those of the greenstone proper is still unclear because of poor exposure. Thus, some may regard the metamorphic sequence as the basement unit, and others may consider that the metamorphic sequence overlain unconformably the greenstone belt. This rock gives CHIME monazite age of 534 ± 10 Ma and xenotime age of 530 ± 32 Ma. The well-defined isochrons with no indication of older and younger ages (Fig 4a,b) suggest a single-stage crystallization of monazite and xenotime during the kyanite-sillimanite type metamorphism ca. 530 Ma ago. We, therefore, consider that the paragneisses at Maevatanana represent the northern extension of the ca. 530 Ma metamorphic rocks at Ihosy in the southern sector. Presumably the central NS trending ductile shear zone of Pan-African age is much wider than has been thought (Windley et al., 1994).

The high-grade metamorphism at ca. 530 Ma in Madagascar appears to be essentially synchronous with the granulite facies metamorphism in the south of the so-called Achankovil shear zone in southern India (539 ± 20 Ma, Santosh et al., 1992; 558 ± 11 Ma, Choudhary et al., 1992; 527 ± 10 Ma, Bindu et al., 1996). Bindu et al. (1996) also reported a 640 ± 30 Ma CHIME age for detrital zircon from the cordierite charnockite sample that gives 527 ± 10 Ma CHIME monazite age. This clearly shows that gneisses in southernmost India are not the

polymetamorphosed Proterozoic complex; they formed newly in the Cambrian from post-640 Ma protolith. Similar Cambrian high-grade paragneisses derived from post-620–760 Ma sediments occur in the Yamato Mountains and the Sør Rondane Mountains in East Antarctica (Shiraishi et al., 1994; Asami et al., 1997).

It has been known that metamorphic rocks in Sri Lanka bear many similarities with those in southernmost India and East Antarctica (Yoshida et al., 1992; Shiraishi et al., 1994). We, therefore, consider that the Cambrian (ca. 530 Ma) metamorphic rocks in Madagascar, southernmost India, Sri Lanka and East Antarctica constituted a single metamorphic terrain that can be linked directly to the collision of East and West Gondwana.

ACKNOWLEDGEMENTS

We acknowledge Prof. M. Adachi of Nagoya University for his enlightening comments. One of us, MI, would like to express his deep gratitude to Dr. R.A. Rambeloson of the University of Antananarivo, Dr. L.D. Ashwal of Rand Afrikaans University, Dr. S. Muhongo of the University of Dar-es-Salaam and Dr. M. Yoshida of Osaka City University for very kind coodination of UNESCO-IUGS-IGCP-348/368 International Joint Field Workshop held in Madagascar in 1997. Journal reviews by Prof. Y. Nakai and an anonymous referee provided a constructive framework which vastly improved the manuscript.

REFERENCES

Adachi, M. and Suzuki, K. (1992) A preliminary note on the age of detrital monazites and zircons from sandstones in the Upper Triassic Nabae Group, Maizuru terrane. *Mem. Geol. Soc. Japan*, **38**, 111–120.

Asami, M., Suzuki, K. and Adachi, M. (1997) Th, U and Pb analytical data and CHIME dating of monazites from metamorphic rocks of the Rayner, Lüzow-Holm, Yamato-Belgica and Sør Rondane complexes, East Antarctica. *Proc. NIPR Symp. Antarct. Geosci.*, **10**, 130–152.

Bindu, R.S.I., Suzuki, K., Yoshida, M. and Santosh, M. (1996) Pan-African tectonothermal events in East Gondwana land: Evidence from south Indian granulite using CHIME age dating. *Abst. 16th Symp. Antarct. Geosci. NIPR, Japan*, 66–67.

Choudhary, A., Harris, K., Van Calsteren, P., and Hawkesworth, C.J. (1992) Pan-African charnockite formation in Kerala, South India. *Geol. Mag.*, **129**, 257–264.

Kröner, A., Braun, I. and Jaeckel, P. (1996) Zircon geochronology of anatectic melts and residues from a high-grade pelitic assemblage at Ihosy, southern Madagascar: evidence for Pan-African granulite metamorphism. *Geol. Mag.*, **133**, 311–323.

Parrish, R.R. (1990) U-Pb dating of monazite and its application to geological problems. *Can. J. Earth Sci.*, **27**, 1431–1450.

Santosh, M., Kagami, H., Yoshida, M and Nanda-Kumar, V. (1992) Pan-African charnockite formation in East Gondwana: geochronologic (Sm-Nd and Rb-Sr) and petrogenetic constraints. *Bull. Indian Geol. Assoc.*, **25**, 1–10.

Shiraishi, K., Ellis, D.J., Hiroi, Y., Fanning, C.M., Motoyoshi, Y. and Nakai, Y. (1994) Cambrian orogenic belt in East Antarctica and Sri Lanka: impricatons for Gondwana assembly. *J. Geol.*, **102**, 47–65.

Suzuki, K. and Adachi, M. (1991a) Precambrian provenance and Silurian metamorphism of the Tsubonosawa paragneiss in the South Kitakami Terrane, Northeast Japan, revealed by the chemical Th-U-total Pb isochron ages of monazite, zircon and xenotime. *Geochemical J.*, **25**, 357–376.

Suzuki, K. and Adachi, M. (1991b) The chemical Th-U-total Pb isochron ages of zircon and monazite from the Gray Granite of the Hida terrane, Japan. *J. Earth Sci., Nagoya Univ.*, **38**, 11–37.

Suzuki, K. and Adachi, M. (1994) Middle Precambrian detrital monazite and zircon from the Hida gneiss on Oki-Dogo Island, Japan: their origin and implication for the correlation of the basement gneiss of Southwest Japan and Korea. *Tectonophysics*, **235**, 277–292.

Suzuki, K., Adachi., M. and Kajizuka, I. (1994) Electron microprobe observations of Pb diffusion in metamorphosed detrital monazites. *Earth Planet. Sci. Lett.* **128**, 391–405.

Windley, B.F., Razafiniparany, A., Razakamanana, T. and Ackermand, D. (1994) Tectonic framework of the Precambrian of Madagascar and its Gondwana connections: a review and reappraisal. *Geol. Rundsch.* **83**, 642–659.

Yoshida, M., Funaki, M. and Viyanaga, P.W. (1992) Proterozoic to Mesozoic East Gondwana: the juxtaposition of India-Sri Lanka and Antarctica. *Tectonics*, **11**, 381–391.